Acta Materialia 125 (2017) 136–144

Contents lists available at ScienceDirect

Acta Materialia

journal homepage: www.elsevier.com/locate/actamat

Full length article

Interface dynamics in one-dimensional nanoscale Cu/Sn couples

Qiyue Yin [a], Fan Gao [b], Zhiyong Gu [b], Jirui Wang [b], Eric A. Stach [c], Guangwen Zhou [a, *]

[a] Department of Mechanical Engineering & Materials Science and Engineering Program, State University of New York at Binghamton, NY, 13902, USA
[b] Department of Chemical Engineering, University of Massachusetts Lowell, Lowell, MA, 01854, USA
[c] Center for Functional Nanomaterials, Brookhaven National Laboratory, Upton, NY, 11973, USA

ARTICLE INFO

Article history:
Received 24 April 2016
Received in revised form
13 November 2016
Accepted 20 November 2016

Keywords:
Cu-Sn
Diffusion
Cu_6Sn_5
Cu_3Sn
Interface
Transmission electron microscopy

ABSTRACT

The isothermal metallurgical reaction in two-segmented Cu-Sn nanowires results in the formation of a $Sn/Cu_6Sn_5/Cu_3Sn/Cu$ sandwich structure. In-situ transmission electron microscopy is used to study how Cu_6Sn_5/Sn and Cu/Cu_3Sn interfaces propagate and change shape during the intermetallic compound growth. The Cu_6Sn_5/Sn interface is observed to evolve from an inclined configuration to a vertical, edge-on configuration with the propagation of the Cu_6Sn_5 phase towards the Sn segment. The Cu/Cu_3Sn interface also becomes less inclined as it propagates toward the Cu segment. This interface evolution is driven by the minimization of the interface energy associated with minimizing the interface area associated with the edge-on interface. The Kirkendall void growth induces the breakage of the Cu segment and results in the $Cu_3Sn \rightarrow Cu_6Sn_5$ transformation with the final $Sn/Cu_6Sn_5/void/Cu$ sandwich structure.

1. Introduction

Numerous nanostructured materials such as nanoparticles, nanotubes, nanowires and nanocomposites have been synthesized and developed in the past two decades. There is, however, a lack of efficient and effective methods for joining and interconnecting individual nanostructured units, which impedes the efficient manufacture of nanoelectronics and nanoscale devices. In contrast, conventional interconnect formation by soldering is extremely robust when compared to other techniques such as controlled growth, irradiation and atomic diffusion [1–7]. Nanowires are one of the most studied one dimensional (1D) nanostructures, as they can function as basic electronic circuit elements or be assembled and integrated into 1D, 2D, or 3D functional structures. As a result, they have great potential in applications such as electronics, sensors and biomedical devices [8–12]. The efficient and robust creation of nanowires with functional nanocomponents and nanosolder segments could serve as a basic building block for nanoelectronic integration.

Lead-free solders are now used to replace traditional tin/lead (Sn/Pb) solders due to the hazardous threats of Pb. Different Pb-free solder nanowires, such as Sn, In, Sn-Cu, Sn-Ag, Sn-Ag-Cu have been synthesized using electrodeposition in nanoporous templates [13–16]. However, fundamental understanding of wetting, diffusion, intermetallic compound (IMC) formation and its associated interface motion between the nanosolder and functional nanocomponents during the soldering reaction of the nanowires is still very limited. An in-depth understanding of these fundamental properties is essential for better control and improvement of the process of nano-soldering and the formation of reliable nanoscale interconnects. By choosing two-segment Cu-Sn nanowires as a model system, in which Sn acts as the solder element and Cu serves as a functional element, we seek to elucidate such fundamental properties. We employ in-situ transmission electron microscopy (TEM) to investigate the IMC growth-induced interface propagation and the Kirkendall void formation during the isothermal solid state soldering/reactive diffusion process.

2. Experimental

The Cu-Sn two-segment nanowires were fabricated by room-temperature sequential electrodeposition assisted with polycarbonate nanoporous membrane templates (Whatman). Cu was deposited first using a commercial Cu plating electrolyte (Cu U-bath RTU, Technic, Inc) with the current controlled at 2 mA/cm^2. After Cu plating, the Sn layer was electroplated with commercial Sn

* Corresponding author.
E-mail address: gzhou@binghamton.edu (G. Zhou).

http://dx.doi.org/10.1016/j.actamat.2016.11.051
1359-6454/

plating electrolyte (Sn concentrate with make-up solutions, Technic, Inc.) with the current controlled at 18 mA/cm^2. After the electroplating, the polycarbonate membrane was dissolved in dichloromethane to release the nanowires into the solvent. Details of the synthesis of the nanosolders can be found from previous work [3,16,17]. The as-prepared Cu-Sn nanowires were kept as a suspension in ethanol. TEM samples were prepared by the powder sample preparation method with ultrasonic dispersion followed with drop casting onto a lacey carbon film supported by Mo grid, which was then mounted onto a Gatan heating holder with rapid heating capability using a Gatan hot-stage temperature controller. In-situ transmission electron microscopy (TEM) and scanning TEM (STEM) observations of the metallurgical reaction in the Cu-Sn two-segment nanowires were performed using a JEOL JEM2100F operated at 200 kV equipped with an x-ray energy dispersive spectrometer (XEDS) (Oxford Energy TEM 250). Due to relatively long acquisition time for STEM imaging, time-series XEDS in the scanning nanoprobe mode (probe diameter of ~1 nm) was used to track the interface migration and composition variation during the isothermal metallurgical reaction in the Cu/Sn couples. The STEM-XEDS line scanning was acquired at 200 °C and the acquisition time was 25 s after signal to noise optimization.

3. Results and discussion

Cu and Sn two segments were sequentially electrodeposited in the form of nanowires for studying the metallurgical reaction between Cu and Sn. Fig. 1(a) shows a backscattered scanning electron microscope (SEM) image of the as-synthesized Cu-Sn nanowires, where the bright segments of the nanowires correspond to the Sn segments, while the slightly darker segments correspond to the Cu segments due to the heavier atomic number of Sn when compared with Cu. Fig. 1(b) shows a TEM bright-field (BF) image of an as-synthesized Cu-Sn two segmented nanowire; inset is a higher magnification TEM image showing the presence of an amorphous native oxide layer wrapped around the whole nanowire surface. The amorphous layer around the Sn and Cu segments has the similar thickness of about 5 nm. From the elemental mapping, the oxide layer located on Cu segment is CuO_x whereas that around the Sn segment is SnO_x. These oxide layers are found to be stable at elevated temperature of 200 °C examined. Fig. 1(c) illustrates a STEM high angle annular dark field (HAADF) image of the nanowire, which shows the bright contrast for the Sn segment while slightly darker contrast for the Cu segment, consistent with the contrast feature with the backscattered SEM image shown in Fig. 1(a). The corresponding XEDS elemental mapping of the nanowire is shown in Fig. 1(d and e) from which the Sn and Cu segments can be easily identified. Quantitative spot-mode EDS analyses indicate that the Sn segment has ~10 at. % Cu whereas the Cu segment has ~1 at. % Sn. The structure of the two segments is confirmed by electron diffraction as Cu and Sn, respectively. Both the SEM and S/TEM images indicate that the as-prepared Cu-Sn nanowires are continuous without any void or gap between the Cu and Sn segments.

To identify the structure of the IMC formed during the isothermal solid state diffusion and soldering reaction, a single Cu-Sn nanowire was selected for isothermally heating at 200 °C until the solder reaction reached an equilibrium state, which was monitored by obtaining diffraction patterns from the heated nanowire for structure analysis. The isothermal temperature of 200 °C was chosen because it is below the melting point of Sn, while still giving sufficiently fast kinetics for the solid state reaction [18], thereby facilitating the in-situ TEM observations. Fig. 2(a) is a TEM image of a Cu-Sn nanowire after isothermal heating at 200 °C for 4 min, which shows the formation of a Kirkendall void in the Cu segment due to the greater out-diffusion flux of Cu from the Cu segment than the in-diffusion flux of Sn [19]. Fig. 2(b) is an SAED (selected area electron diffraction) pattern taken from the area

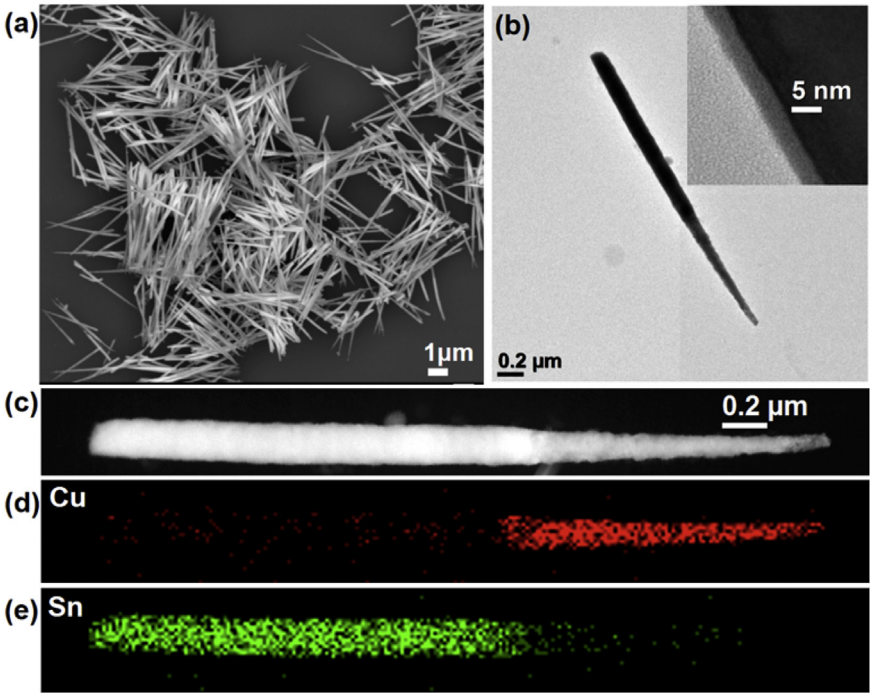

Fig. 1. As-prepared Cu-Sn two segmented nanowires by a template assisted electrodeposition method. (a) A SEM image of Cu-Sn two segmented nanowires; (b) TEM BF image of a Cu-Sn nanowire; (c) STEM-HAADF image of the Cu-Sn nanowire; (d, e) STEM EDS elemental mapping of the Cu-Sn nanowire with the Cu map in red and Sn map in green. (For interpretation of the references to colour in this figure legend, the reader is referred to the web version of this article).

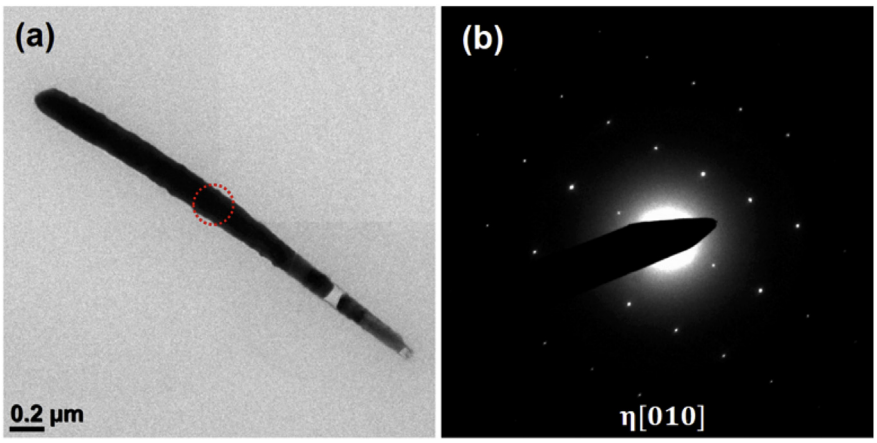

Fig. 2. Formation of the Cu_6Sn_5 IMC from the isothermal heating of the Cu-Sn two-segmented nanowire at 200 °C. (a) TEM image of a Cu-Sn two segmented nanowire after the isothermal heating at 200 °C for 4 min; (b) electron diffraction pattern taken from the selected area encircled by the red dash line as shown in (a) showing the η-Cu_6Sn_5 structure. (For interpretation of the references to colour in this figure legend, the reader is referred to the web version of this article).

marked by the red dash circle indicated in Fig. 2(a) while the sample was held at 200 °C, which can be indexed well with the zone axis of [010] of the η-Cu_6Sn_5 structure [20]. By checking dozens of Cu-Sn two segmented nanowires after it reached the equilibrium/final state with the isothermal heating at 200 °C, it was confirmed that most of the IMCs formed at 200 °C have the η-Cu_6Sn_5 with very few cases of the formation of η′-Cu_6Sn_5 under the same heating condition.

TEM imaging is a two-dimensional (2D) projection view of a 3D object along the direction of the transmitted electron beam. By taking into account this effect and the cylindrical morphology of the nanowire, Fig. 3(a) shows a 3D schematic view of a typical inclined interface between the two adjacent different phases. Purple and violet represent the Cu_6Sn_5 segment and the remaining Sn segment respectively, and the black curve denotes their interface plane. The Cartesian coordinate x, y, z of the nanowire is also shown in Fig. 3(a) for the convenience of description and discussion. To demonstrate this wedge-shape interface between the two phases, we can visualize the change in the interface morphology of a reacted Cu-Sn nanowire by tilting the TEM viewing direction from the x direction to the z direction. Fig. 3(b) shows a TEM BF image of a nanowire viewed from the x direction. As shown schematically in the inlet of Fig. 3(b), the interface is projected as an inclined straight line under this TEM viewing condition, which matches well with the TEM-BF image (Fig. 3(b)) of a reacted Cu-Sn nanowire with the incident e-beam parallel to the x direction. Fig. 3(c) presents an electron diffraction pattern from the area encircled by the white dashed circle, as indicated in Fig. 3(b), which can be indexed well as Sn [111]. The electron diffraction pattern of the area encircled by the red dashed circle as indicated in Fig. 3(b) is shown in Fig. 3(e), which matches well with η-Cu_6Sn_5 $[\bar{1}10]$. Due to the diffraction effect, with the η phase aligned on the zone axis, the η phase appears dark while the Sn segment appears brighter in Fig. 3(b). The Sn/η phase interface appears as a straight and inclined line, as marked by a red dashed oval in Fig. 3(b). By tilting the nanowire, we can set the nanowire to be aligned with the z direction parallel to the incident e-beam. As marked by the red dashed oval in Fig. 3(d), the projected interface profile viewed along the z direction appears now as a curved line, which agrees well with the inset schematic projection view in Fig. 3(d). As shown in Fig. 3(d), the upper region outlined by the white dashed line is brighter than the lower part, which corresponds to a thinned region due to the depletion of Sn in the parent Sn segment. It can be seen from Fig. 3(b, d) that the thinned region extends across the Cu_6Sn_5/Sn interface to the Cu_6Sn_5 grain, suggesting that the thinned region is formed before the Sn/Cu_6Sn_5 interface propagates into this area.

To study the compositional variation accompanying the diffusion and dynamics of intermetallic compound growth and propagation during the Cu/Sn metallurgical reaction, a single Cu-Sn two-segmented nanowire was selected for in-situ heating STEM observation combined with XEDS elemental line scan. In-situ time-sequence series of STEM BF images and the line scan concentration profiles of a Cu/Sn two-segmented nanowire with the as-prepared state and during the isothermal heating at 200 °C are shown in Fig. 4. Noticeable void formation occurs in the Cu segment after ~123 s of the isothermal heating, which is caused by faster diffusion of Cu into the Sn segment than Sn diffusion into the Cu segment (i.e., Kirkendall effect). The Kirkendall void grows with the continued heating, which results in the breakage in the Cu segment at ~568 s. Although the void cuts off the diffusion path and thus the supply of Cu atoms from the right end of the nanowire to the left end, Cu atoms in the remnant Cu segment on the left side of the void continue to diffuse and react with the Sn segment, as shown in the STEM BF image at 902 s in Fig. 4(e). After the remaining Cu segment on the left side of the void is completely consumed, the nanowire does not show any observable changes with subsequent time at this temperature.

The elemental composition profiles by XEDS linescan taken along the length direction of the nanowire at the isothermal annealing time of 123 s, 485 s, 568 s, 902 s, and 1638 s are also shown in Fig. 4, respectively. Each concentration profile can be divided into five different regions, as marked by violet, purple, blue, green and orange in Fig. 4(b). Region I, which ranges from $x = 0$ to $x = x_1$ and is highlighted in violet in Fig. 4(b), corresponds to the Sn segment. Region V, which ranges from x_4 to the right end of the nanowire, represents the Cu segment as indicated by the orange area in Fig. 4(b). The composition profiles of Cu and Sn show the overlapped plateau in Region II, as defined between x_1 and x_2 and marked by the purple area in Fig. 4(b), which corresponds to the Cu_6Sn_5 segment that results from the Cu-Sn reaction. The Cu_6Sn_5 has a narrow compositional range (43.5–44.5 atomic % Sn) [20,21], which matches well with the measured composition in Region II. The composition profiles of Cu and Sn show the overlapped plateau in Region III with ~75 at. % Cu, as defined between x_2 and x_3 and marked by the blue area in Fig. 4(b), which probably corresponds to the formation of a small Cu_3Sn segment (as confirmed by electron diffraction shown in Fig. 5). The most noteworthy feature of the composition profiles is in Region IV as marked by color in Fig. 4(b),

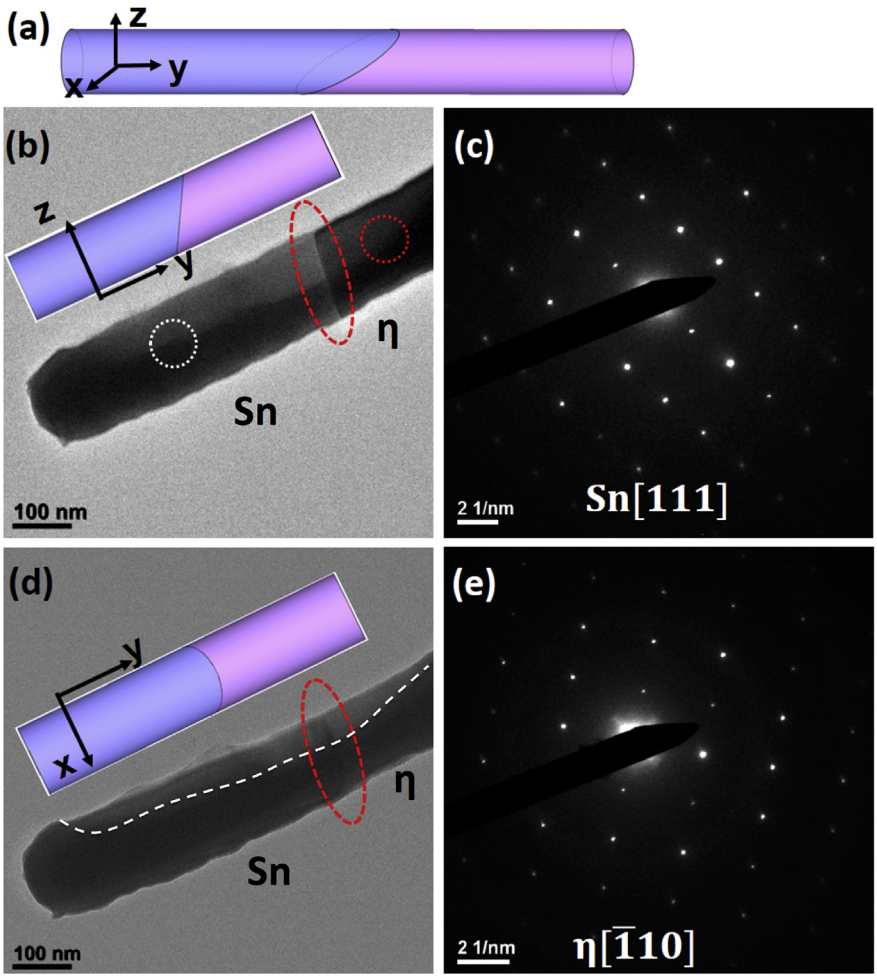

Fig. 3. Visualization of the inclined interface projected along x or z direction. (a) 3D schematic of an inclined interface between two adjacent phases in a nanowire; (b) the Sn/η interface projected along x direction, as encircled by the oval dash line, inlet is the schematic projection view of the phase interface with beam parallel to x direction; (c) the electron diffraction taken from area encircled by the white dash line as shown in (a), and (d) the Sn/η interface is projected along z, acquired by large α tilting change, inlet is the schematic projection view of the phase interface with beam parallel to z direction; (e) the electron diffraction from area encircled by the red dash line as shown in (b). (For interpretation of the references to colour in this figure legend, the reader is referred to the web version of this article).

which is Cu-rich with a gradually increasing gradient of the Cu concentration.

To find out whether Cu_3Sn exists during the Cu-Sn reaction we performed additional in-situ heating experiments with different Cu-Sn nanowires. We used electron diffraction to monitor the structure evolution of Cu-Sn couples with prolonged heating at 200 °C. As shown in Fig. 5, a single two-segment Cu-Sn nanowire with a longer Sn segment is shown from the experiment: the red dashed line indicates the position of the Cu/Sn interface in the as-prepared nanowire (Fig. 5(a)). After rapid ramping to 200 °C, the sample was held at this temperature for the solid-state reaction. Fig. 5(b) is a BF image of the nanowire after 300 s of the isothermal heating, which shows the formation of a Kirkendall void in the Cu segment near the interface region. Fig. 5(c) is an electron diffraction pattern from the region indicated by the white dashed circle in Fig. 5(b). The diffraction spots with the d spacing of 4.8 Å, which exclusively correspond to ε-Cu_3Sn (100), are clearly visible as indicated by red arrows in Fig. 5(c). From the in-situ TEM analysis, we can draw the conclusion that the ε-Cu_3Sn phase does exist before the Kirkendall void growth breaks the nanowire.

The temporal evolution and motion of the interfaces formed from IMC growth during the Cu-Sn metallurgical reaction can be revealed by tracking the temporal evolution of the concentration profile across the interface during the isothermal annealing of the nanowires. The chemical compositional profile in Fig. 4 demonstrates that the ε-Cu_3Sn and Cu segments overlap at their inclined interface when the scanning electron probe is aligned along the z direction of the nanowire, as illustrated in Fig. 3(a). Region II - as highlighted by purple in Fig. 4(b) - can be taken as the Cu_6Sn_5 segment with the length Lη as (x_2-x_1). Region III as highlighted by blue in Fig. 4(b) corresponds to the ε-Cu_3Sn segment with the length Lε as (x_3-x_2). The width of the overlapping region of the ε-Cu_3Sn and Cu segments along their inclined interface can be identified by $w = x_4$-x_3, which is also marked as region IV by green in Fig. 4(b). The temporal evolution of the lengths (Lη and Lε) of the η and ε phase and their interface widths (w) can be determined from the in-situ STEM EDS measurements shown in Fig. 4 and the results are given in Fig. 6 with a 3D schematic illustration showing the definition of each term in the plot. By tracking the growth or shrinkage of these regions we can follow the propagation and morphological evolution of the interfaces during the growth of the ε-Cu_3Sn and η-Cu_6Sn_5 segments.

Fig. 6 shows the length evolution of the ε-Cu_3Sn and η-Cu_6Sn_5 segments and the width evolution of the inclined interface

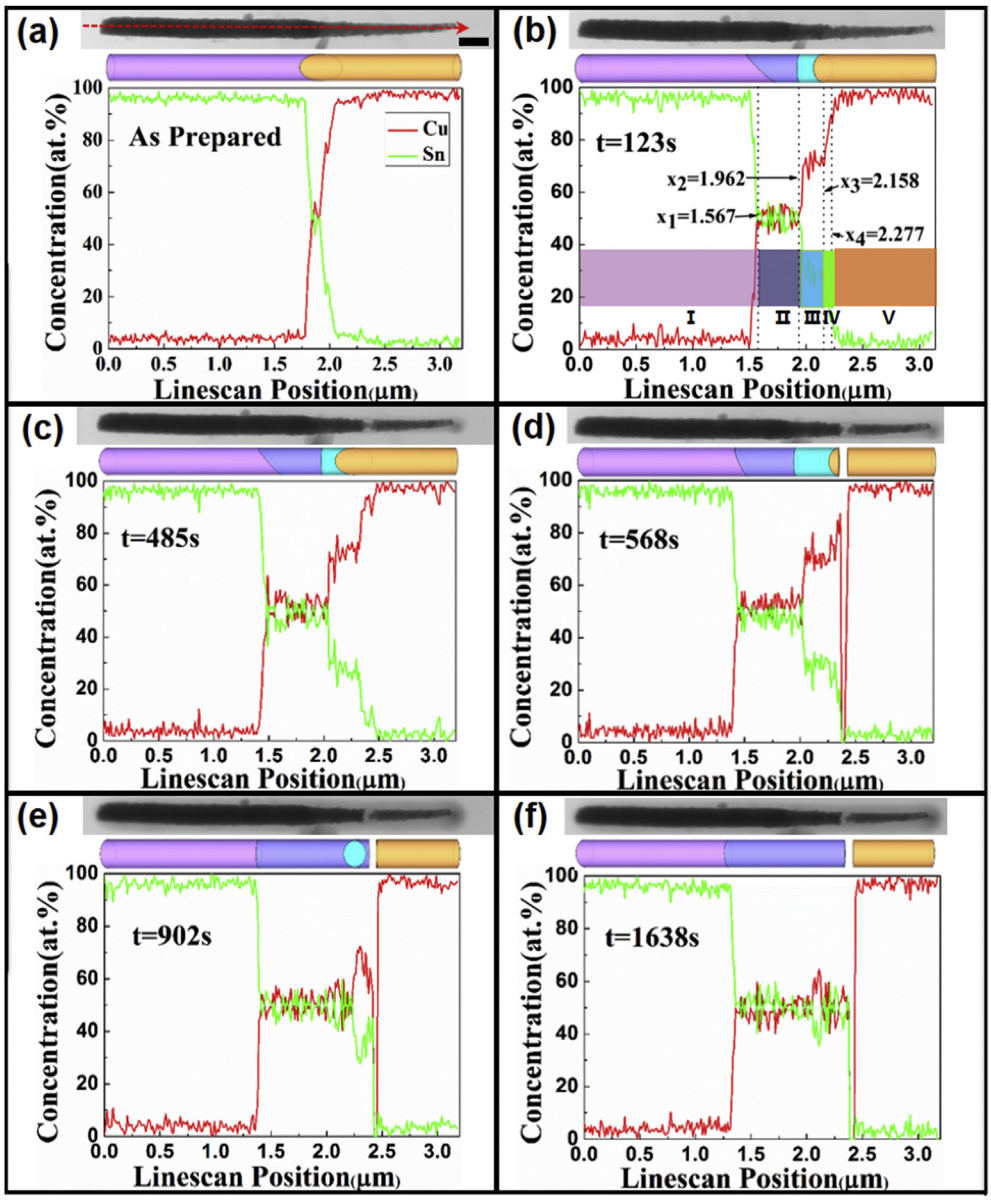

Fig. 4. Time series STEM XEDS elemental linescans during in-situ isothermal heating at 200 °C. (a) STEM BF image and concentration profile along the length of an as-prepared Cu-Sn nanowire as marked by the red dashed line on the STEM image; (b, c, d, e, f) STEM images and concentration profiles along the length of the nanowire at 200 °C for 123 s, 485 s, 568 s, 902 s and 1638 s, respectively. The scale bar is 200 nm. The insets illustrate the 3D schematic of the interface shift and propagation determined from *in situ EDS* measurements of the composition. (Violet, Purple, Blue and Orange represent Sn, Cu_6Sn_5, Cu_3Sn and Cu, respectively.). (For interpretation of the references to colour in this figure legend, the reader is referred to the web version of this article).

between the ε-Cu_3Sn and Cu segments. As shown by the black line with solid black squares in Fig. 6, the length of the Cu_6Sn_5 segment (Lη), increases with time, indicating that the Cu_6Sn_5 segment grows continuously during the isothermal reaction. The red line with red solid circles in Fig. 6 represents the length of the ε-Cu_3Sn segment, which increases with time before the Kirkendall void growth breaks the nanowire at t = 568 s. We then see that the ε-Cu_3Sn segment shrinks and transforms to Cu_6Sn_5 after the Kirkendall void growth breaks the Cu segment and cuts off the Cu supply. The width of the Cu_3Sn/Cu interface (shown by the red line with hollow triangles in Fig. 6) decreases with time, indicating that the ε-Cu_3Sn/Cu interface becomes less inclined over time (a vertical interface has an interface width w = 0) until the void growth breaks the nanowire. As shown in the concentration profile in Fig. 4(d), region IV is still Cu-rich as compared to region III after the breakage of the Cu segment, indicating that there is a small remnant Cu segment on the left of the Kirkendall void, as shown by the 3D schematic inlet in Fig. 4(d). Incoming diffusing Sn atoms (from the Sn end) react with the ε-Cu_3Sn segment and the remnant Cu to form Cu_6Sn_5, as illustrated by the 3D schematic inlet in Fig. 4(e). With the continued isothermal solid reaction, the remnant Cu on the left of the Kirkendall void is completely consumed at around t = 1640 s. This in turn leads to the drop of the Cu concentration and the increase of the Sn concentration to the level similar to region II (Fig. 4(e and f)) because the ε-Cu_3Sn segment gradually transforms to the η-Cu_6Sn_5 phase. The time sequence of the EDS composition profiles (Fig. 4(d, e, f)) shows that the concentrations of both Cu and Sn drop to zero across the Kirkendall void, suggesting that the void remains there after it breaks the Cu segment and shuts off the diffusion pathways with the Cu segment on the right end of the void. However, in

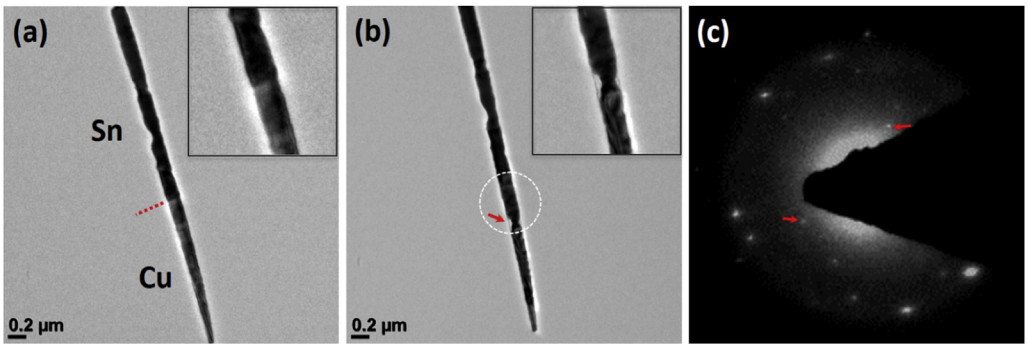

Fig. 5. (a) Bright-field (BF) image of an as-prepared Cu-Sn two-segmented nanowire, the red dashed line indicates the Cu/Sn interface, inset is a magnified view of the interface region; (b) BF image of the nanowire showing the formation of a Kirkendall void in the Cu segment after 300 s of the isothermal heating, inset is a magnified view of the Kirkendall void region; (c) SAED obtained from the region indicated by the white dashed circle in (b). (For interpretation of the references to colour in this figure legend, the reader is referred to the web version of this article).

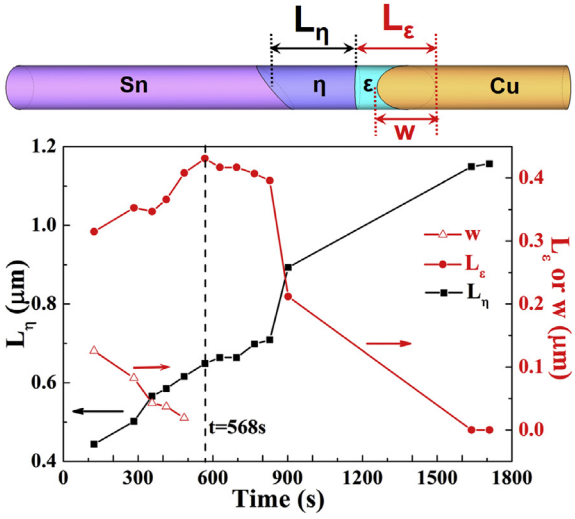

Fig. 6. Evolution of the lengths of the η-Cu_6Sn_5 segment (L_η) and the ε-Cu_3Sn segment (L_ε) and the width (w) of the Cu/Cu_3Sn interface. Upper panel: 3D schematic illustrating how L_η, L_ε, and w are defined in the EDS measurement shown in Fig. 4.

contrast with the overlapped Cu and ε-Cu_3Sn region, with beam scanning along the length of the nanowire, the Sn/Cu_6Sn_5 interface is positioned in a scenario with beam parallel to x direction, as depicted in Fig. 3(b). Therefore, the concentration profile across the η-Cu_6Sn_5/Sn interface does not tell whether the η-Cu_6Sn_5/Sn interface configuration has changed over time during the Cu_6Sn_5 growth. As shown below, we know that the η-Cu_6Sn_5/Sn interface evolves from an inclined configuration into a vertical, edge-on configuration.

With the x direction of the nanowire aligned along the incident e-beam as illustrated in Fig. 3(b), we can directly observe the dynamic propagation of the interface during the isothermal metallurgical reaction. Fig. 7(a) shows a time series of in-situ TEM images of a Cu-Sn two-segment nanowire isothermally held at 200 °C. As seen in Fig. 7(a), a Kirkendall void starts to become visible in the Cu segment after ~ 60 s of annealing. With continued time at this temperature, the void grows and shifts to the left side, implying the diffusive flux of Cu atoms toward the right end. Our in-situ TEM observations show that sufficient Cu_6Sn_5 has developed after ~60 s of annealing. Meanwhile, the continued void growth leads to the breakage of the nanowire in the Cu segment as a result. Although the void cuts off the supply of Cu atoms from the Cu segment at the left end, the unreacted Cu segment on the right side of the void (as indicated by the black arrow in Fig. 7(a) at t = 750 s) continues to react with incoming diffusing Sn atoms until it is completely consumed, as shown in the image after 1140 s of annealing. The dynamic motion of the Cu_6Sn_5/Sn interface is followed by the time sequence of in-situ TEM images shown in Fig. 7(a). The red arrows indicate the position of the interface at the moment indicated in Fig. 7(a). It can be noted that the interface not only shifts toward the right, accompanying the growth of the η-Cu_6Sn_5 segment but also changes gradually in its morphology from an initially inclined configuration to a vertical one with continued annealing. The area (S_i) of an inclined interface can be calculated from the TEM images by measuring the width (w) of the overlapping region of the Cu_6Sn_5 and Sn segments across their interface. The area of this inclined interface can be calculated as $S_i = (\pi R/2)\sqrt{(w^2 + 4R^2)}$, where w is the width of the overlapping phase region within the inclined interface and R is the radius of the nanowire. S_i decreases with w as the interface becomes less inclined. When the interface becomes vertical, w is zero, the interface reaches a configuration with the minimum interface area ($S_i = \pi R^2$). Such evolution in the interface configuration can be driven by the interfacial energy, for which the vertical interface configuration corresponds to the interface geometry with the minimum total interface energy. As shown in Fig. 7(a), the η-Cu_6Sn_5/Sn interface becomes nearly vertical after 220 s of the reaction, from which we can accurately determine the migration distance ($\Delta\xi_{\eta/Sn}$) by the η-Cu_6Sn_5/Sn interface. Our in-situ TEM measurements show that $\Delta\xi_{\eta/Sn}$ follows a parabolic time dependence of the interface movement (Fig. 7(b)), indicating that the interface migration is controlled by the interdiffusion of the reactants (Cu and Sn). This is consistent with the derivation by Kidson [22] with the application of Fick's first law of diffusion to polyphase diffusion in binary systems.

The phase evolution induced by the isothermal annealing of the Cu-Sn nanowire shown in Fig. 7(a) was characterized by electron diffraction. Fig. 8(b, c) show the electron diffraction patterns taken from the different areas (denoted as "B" and "C in Fig. 8(a)) of the nanowire after 1140 s of heating at 200 °C. Fig. 8(d, e) are the simulated diffraction patterns corresponding to the experimental electron diffractions of Fig. 8(b, c), respectively. Area "B" has the diffraction pattern indexed as η-Cu_6Sn_5 with orientation [011]. The diffraction pattern from area "C" matches well with pure Sn [102]. Between areas "B" and "C" is the interface between the η-Cu_6Sn_5 and Sn segment. The structure analysis is consistent with the XEDS elemental mapping shown in Fig. 9(a–c) and the compositional linescan profile shown in Fig. 9(d). Both the diffraction and XEDS

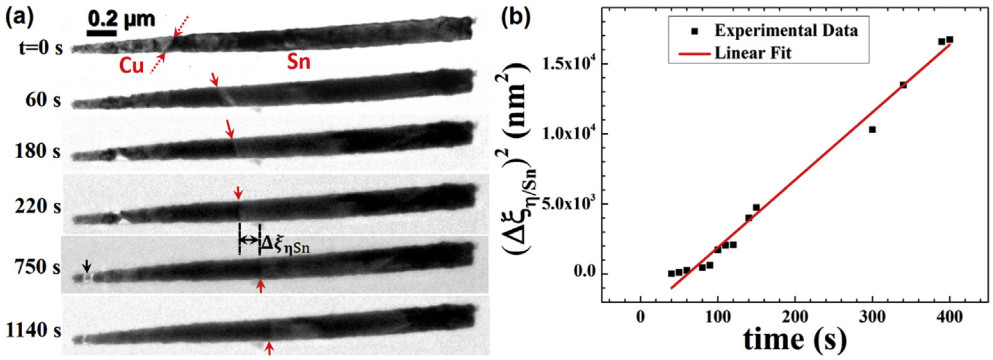

Fig. 7. **(a)** In-situ TEM BF images of the Cu_6Sn_5/Sn interface propagation induced by the metallurgical reaction in a Cu-Sn two-segment nanowire during the isothermal heating at 200 °C. The area encircled by the red dash line indicates the temporal evolution of the interface between the η-Cu_6Sn_5 phase (left) and Sn (right) from an initially inclined configuration to a vertical (edge-on) one after ~ 220 s and then stays vertical while it propagates into the Sn segment with prolonged time (750 s and 1140 s); (b) Linear regression fitting of the $(\Delta\xi_{\eta/Sn})^2$ with time, indicating the parabolic time dependence of the interface propagation. (For interpretation of the references to colour in this figure legend, the reader is referred to the web version of this article).

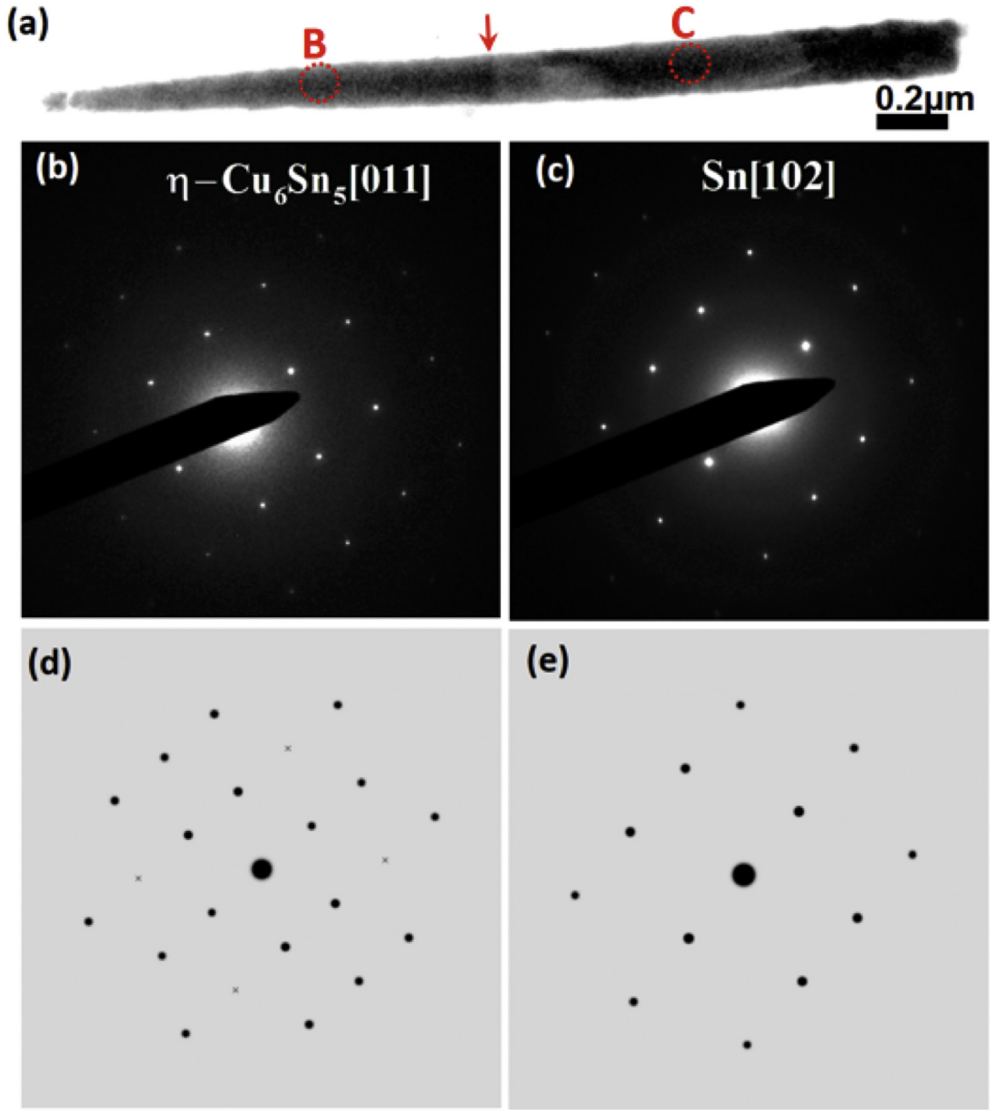

Fig. 8. Structure Characterization of the nanowire in Fig. 7 after withholding at 200 °C for 1140s. (a) TEM BF image of the nanowire isothermally heated at 200 °C for 1140s, the dash line represents the η/Sn interface; (b) SAED from the encircled area "B", as denoted in Fig. 8a; (c) SAED pattern from the encircled area "C", as denoted in Fig. 8a; (d, e) Simulated diffraction patterns corresponding to the SAED pattern of Fig. 8(b, c), respectively.

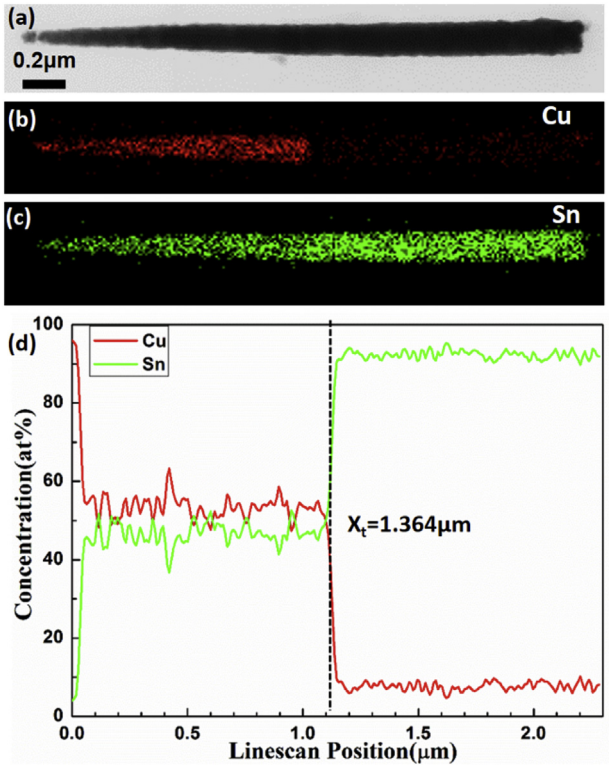

Fig. 9. Elemental mapping of the nanowire as shown in Fig. 7 after isothermally heated at 200 °C for 1140 s (a) STEM BF image of the nanowire; (b, c) Elemental mapping; (d) Line scan profile along the length of the nanowire.

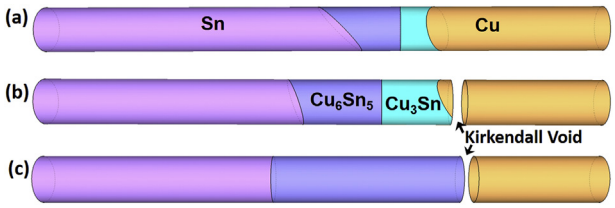

Fig. 10. Schematic showing the formation of a Sn/Cu_6Sn_5/Cu_3Sn/Cu sandwich structure and the propagation and shape change of the different interfaces during isothermal annealing of a two-segmented Cu-Sn nanowire at 200 °C. The Cu_6Sn_5/Sn interface propagates toward the Sn segment and evolves gradually from being inclined to vertical. The Cu/Cu_3Sn interface becomes less inclined as well. (a) The reaction results in the growth of both Cu_3Sn and Cu_6Sn_5 segments; (b) with prolonged time when the Kirkendall void breaks the nanowire both the Cu/Cu_3Sn and Sn/Cu_6Sn_5 interface is less inclined as compared to (a); (c) with continued isothermal heating after the Kirkendall void cuts off the diffusion path between the Cu and Cu_3Sn segments, the Cu_3Sn segment and the adjacent Cu react with incoming diffusing Sn atoms to form Cu_6Sn_5 until completely consumed. The Sn/Cu_6Sn_5 interface adopts vertical as the stabilized configuration. Termination of the metallurgical reaction results in a Sn/Cu_6Sn_5/void/Cu sandwich structure.

were taken or acquired at 200 °C and they are congruent with the dynamic motion of the phase interface identified in Fig. 7(a).

Our in-situ TEM observations described above show how the propagation and shape of the phase interfaces occur during the isothermal solid reaction. With the x direction of the nanowire parallel to the beam and the projection of the interface as a straight line, the η-Cu_6Sn_5/Sn interface propagates toward the Sn segment and changes gradually from an inclined configuration to a vertical one (see Fig. 7(a)). The propagation of the ε-Cu_3Sn/Cu interface is resolved by the time-sequence of the concentration profiles, which shows that the ε-Cu_3Sn/Cu interface also becomes less inclined until the Kirkendall void growth breaks the Cu segment.

The remaining Cu between the void and Cu_3Sn segment continues to react and form η-Cu_6Sn_5 with incoming diffusing Sn atoms from the Sn end. The Kirkendall void formed in the Cu segment is due to faster diffusion of Cu in the intermetallic phases as compared to that of Sn in the intermetallic compounds. A schematic illustrating the interface migration and the associated temporal evolution of the interface configuration described above is shown in Fig. 10, where the orange, blue, purple and violet represent the Cu, Cu_3Sn, Cu_6Sn_5 and Sn segments, respectively. Fig. 10(a) indicates that the Cu-Sn reaction results in the growth of the η-Cu_6Sn_5 and ε-Cu_3Sn segments between the parent Cu and Sn segments with the formation of three interfaces, i.e., the Sn/Cu_6Sn_5, Cu_6Sn_5/Cu_3Sn, and Cu_3Sn/Cu interfaces, among which the Sn/Cu_6Sn_5 and Cu_3Sn/Cu interfaces are both initially inclined. With the continued isothermal annealing, the Cu/Cu_3Sn interface becomes less inclined until the Kirkendall void breaks the nanowire, the Cu_6Sn_5/Sn interface also evolves to a vertical configuration, as shown in Fig. 10(b). As shown in Fig. 10(c), after the Kirkendall void breaks the wire, Cu_3Sn gradually transforms to Cu_6Sn_5 by reacting with the remnant Cu atoms and incoming diffusing Sn atoms from the Sn end. Some remnant Cu atoms may diffuse through the Cu_6Sn_5 and Cu_3Sn segments to react with Sn for the growth of the Cu_6Sn_5 toward the Sn end until all the remnant Cu atoms are completely consumed.

The interfacial energy plays an important role in understanding not only the wetting behavior between the liquid and the solid, but also the phase transition and associated solid/solid interfaces [23,24]. As shown in Fig. 1, there is an amorphous native oxide layer (~5 nm in thickness) wrapping around the nanowire like a shell. Here we use N to represent the native oxide. With the confinement of this amorphous oxide layer there are seven different types of the interface energy taken into account for the nanowire, i.e., Cu_6Sn_5/Sn, Cu_6Sn_5/Cu_3Sn, Cu/Cu_3Sn, oxide/Cu_6Sn_5, oxide/Cu_3Sn, Cu/oxide, and Sn/oxide. During the solid-state reaction, the oxide/Cu_6Sn_5, oxide/Cu_3Sn, Cu/oxide, and Sn/oxide remain the same configuration and are independent of the interface inclination, and the Cu_6Sn_5/Cu_3Sn interface remains vertical. As described earlier, the areas of the Cu/Cu_3Sn and Cu_6Sn_5/Sn interfaces, can be calculated as $S_i = (\pi R/2)\sqrt{(w^2 + 4R^2)}$. The interface area reaches the minimum with the vertical interface $w = 0$. In addition to the interface area, the interfacial energy density (energy per area) for the Cu/Cu_3Sn and Cu_6Sn_5/Sn interfaces might also change with the inclination, because the orientation and bonding between two crystals affect the interface energy [25,26]. As shown in our in-situ TEM observation, both the Cu/Cu_3Sn and Cu_6Sn_5/Sn interfaces stabilize at the vertical configuration with a minimized interface area, for which the interface energy density is relatively independent of the interface configuration and the interface energy is minimized by minimizing the interfacial area.

4. Conclusions

In-situ TEM has been employed to reveal the propagation and evolution of interfaces in the Sn/Cu_6Sn_5/Cu_3Sn/Cu sandwiched structure during the isothermal metallurgical reaction in two-segmented Cu-Sn nanowires. Both the elemental linescans and TEM imaging from the different view directions of the nanowire confirm the existence of the inclined interfaces. The dynamic process of the Cu_6Sn_5/Sn interface propagation towards the Sn segment and its evolution from an inclined configuration to a vertical configuration is observed. The Cu/Cu_3Sn interface also becomes less inclined as it propagates toward the Cu segment. The driving force that causes the Cu/Cu_3Sn and the Cu_6Sn_5/Sn interface to become vertical or less inclined as their stabilized configuration

is to minimize the interfacial energy. In addition, the observed Kirkendall void formation in the Cu segment demonstrates that the diffusion of Cu in Cu_3Sn and Cu_6Sn_5 is faster than that of Sn in Cu_3Sn and Cu_6Cu_5. The continued Kirkendall void growth in the Cu segment eventually breaks the Cu segment from the nanowire. After the Kirkendall void cuts off the diffusive supply of Cu atoms from the Cu segment, the Cu_3Sn and the adjacent remnant Cu react with the incoming diffusing Sn atoms to form Cu_6Sn_5 until completely consumed, thereby leading to the termination of the metallurgical reaction with a final configuration of Sn/Cu_6Sn_5/void/Cu sandwich structure.

Acknowledgement

This work was supported by the National Science Foundation under NSF Collaborative Research Award Grant CMMI-1233806. Research carried out in part at the Center for Functional Nanomaterials, Brookhaven National Laboratory, which is supported by the U.S. Department of Energy, Office of Basic Energy Sciences, under Contract No. DE-SC0012704.

References

[1] B. Nikoobakht, X. Wang, A. Herzing, J. Shi, Scalable synthesis and device integration of self-registered one-dimensional zinc oxide nanostructures and related materials, Chem. Soc. Rev. 42 (2013) 342–365.
[2] C.-S. Kim, S.-H. Ahn, D.-Y. Jang, Review: developments in micro/nanoscale fabrication by focused ion beams, Vacuum 86 (2012) 1014–1035.
[3] Z. Gu, H. Ye, D. Smirnova, D. Small, D.H. Gracias, Reflow and electrical characteristics of nanoscale solder, Small 2 (2006) 225–229.
[4] L. Zhu, Y. Sun, D.W. Hess, C.-P. Wong, Well-aligned open-ended carbon nanotube architectures: an approach for device assembly, Nano Lett. 6 (2006) 243–247.
[5] X. Li, F. Gao, Z. Gu, Nanowire joining methods, Open Surf. Sci. J. 3 (2011) 91–104.
[6] P. Peng, A. Hu, A.P. Gerlich, Y. Liu, Y.N. Zhou, Self-generated local heating induced nanojoining for room temperature pressureless flexible electronic packaging, Sci. Rep. 5 (2015).
[7] R.-Z. Li, A. Hu, D. Bridges, T. Zhang, K.D. Oakes, R. Peng, U. Tumuluri, Z. Wu, Z. Feng, Robust Ag nanoplate ink for flexible electronics packaging, Nanoscale 7 (2015) 7368–7377.
[8] W. Zhou, X. Dai, T.-M. Fu, C. Xie, J. Liu, C.M. Lieber, Long term stability of nanowire nanoelectronics in physiological environments, Nano Lett. 14 (2014) 1614–1619.
[9] T.-M. Fu, X. Duan, Z. Jiang, X. Dai, P. Xie, Z. Cheng, C.M. Lieber, Sub-10-nm intracellular bioelectronic probes from nanowire–nanotube heterostructures, Proc. Natl. Acad. Sci. 111 (2014) 1259–1264.
[10] X. Duan, R. Gao, P. Xie, T. Cohen-Karni, Q. Qing, H.S. Choe, B. Tian, X. Jiang, C.M. Lieber, Intracellular recordings of action potentials by an extracellular nanoscale field-effect transistor, Nat. Nanotechnol. 7 (2012) 174–179.
[11] Z. Fan, J.C. Ho, T. Takahashi, R. Yerushalmi, K. Takei, A.C. Ford, Y.L. Chueh, A. Javey, Toward the development of printable nanowire electronics and sensors, Adv. Mater. 21 (2009) 3730–3743.
[12] K.-I. Chen, B.-R. Li, Y.-T. Chen, Silicon nanowire field-effect transistor-based biosensors for biomedical diagnosis and cellular recording investigation, Nano Today 6 (2011) 131–154.
[13] H. Zhang, J. Zhang, Q. Lan, H. Ma, K. Qu, B.J. Inkson, N.J. Mellors, D. Xue, Y. Peng, Nanoscale characterization of 1D Sn-3.5 Ag nanosolders and their application into nanowelding at the nanoscale, Nanotechnology 25 (2014) 425301.
[14] K. Qu, H. Zhang, Q. Lan, X. Deng, X. Ma, Y. Huang, J. Zhang, H. Ma, B.J. Inkson, D. Xue, Realization of the welding of individual TiO 2 semiconductor nano-objects using a novel 1D Au 80 Sn 20 nanosolder, J. Mater. Chem. C 3 (2015) 11311–11317.
[15] J.-G. Wang, M.-L. Tian, T.E. Mallouk, M.H. Chan, Microstructure and interdiffusion of template-synthesized Au/Sn/Au junction nanowires, Nano Lett. 4 (2004) 1313–1318.
[16] F. Gao, S. Mukherjee, Q. Cui, Z. Gu, Synthesis, characterization, and thermal properties of nanoscale lead-free solders on multisegmented metal nanowires, J. Phys. Chem. C 113 (2009) 9546–9552.
[17] Q. Yin, F. Gao, Z. Gu, E.A. Stach, G. Zhou, In situ visualization of metallurgical reactions in nanoscale Cu/Sn diffusion couples, Nanoscale 7 (2015) 4984–4994.
[18] K.-N. Tu, Solder Joint Technology, Springer, 2007.
[19] T.-C. Liu, C.-M. Liu, Y.-S. Huang, C. Chen, K.-N. Tu, Eliminate Kirkendall voids in solder reactions on nanotwinned copper, Scr. Mater. 68 (2013) 241–244.
[20] N. Saunders, A. Miodownik, The Cu-Sn (copper-tin) system, Bull. Alloy Phase Diagr. 11 (1990) 278–287.
[21] D. Li, P. Franke, S. Fürtauer, D. Cupid, H. Flandorfer, The Cu–Sn phase diagram part II: new thermodynamic assessment, Intermetallics 34 (2013) 148–158.
[22] G. Kidson, Some aspects of the growth of diffusion layers in binary systems, J. Nucl. Mater. 3 (1961) 21–29.
[23] F. Sommer, R. Singh, E. Mittemeijer, Interface thermodynamics of nano-sized crystalline, amorphous and liquid metallic systems, J. Alloys Compd. 467 (2009) 142–153.
[24] M. Zacharias, P. Streitenberger, Crystallization of amorphous superlattices in the limit of ultrathin films with oxide interfaces, Phys. Rev. B 62 (2000) 8391.
[25] L. Jeurgens, W. Sloof, F. Tichelaar, E. Mittemeijer, Thermodynamic stability of amorphous oxide films on metals: application to aluminum oxide films on aluminum substrates, Phys. Rev. B 62 (2000) 4707.
[26] J. Luo, Grain boundary complexions: the interplay of premelting, prewetting, and multilayer adsorption,, Appl. Phys. Lett. 95 (2009) 071911.